Eur. Phys. J. Plus (2015) **130**: 145
DOI 10.1140/epjp/i2015-15145-x

THE EUROPEAN PHYSICAL JOURNAL PLUS

Regular Article

A neutron pinhole camera for PF-24 source: Conceptual design and optimization

J. Bielecki[a], A. Wójcik-Gargula, U. Wiącek, M. Scholz, A. Igielski, K. Drozdowicz, and U. Woźnicka

Institute of Nuclear Physics Polish Academy of Sciences (IFJ PAN), PL-31-342 Krakow, Poland

Received: 23 January 2015 / Revised: 25 June 2015
Published online: 23 July 2015

Abstract. A fast-neutron pinhole camera based on small-area (5 mm × 5 mm) BCF-12 scintillation detectors with nanosecond time resolution has been designed. The pinhole camera is dedicated to the investigation of the spatial and temporal distributions of DD neutrons from the Plasma Focus (PF-24) source. The geometrical parameters of the camera have been optimized in terms of maximum neutron flux at the imaging plane by means of MCNP calculations. The detection system consists of four closely packed scintillation detectors coupled via long optical fibres to Hamamatsu H3164-10 photomultiplier tubes. The pinhole consists of specially designed 420 mm long copper collimator with an effective aperture of 1.7 mm mounted inside a cylindrical polyethylene tube. The performance of the presented detection system in the mixed (hard X-ray and neutron) radiation field of the PF-24 plasma focus device has been tested. The results of the tests showed that the small-area BCF-12 scintillation detectors can be successfully applied as the detection system of the neutron pinhole camera for the PF-24 device.

1 Introduction

In many experiments with Plasma Focus (PF) devices working with deuterium filling gas, the Doppler energy shift of the neutron spectrum has been observed [1]. This fact indicates the occurrence of the deuterons acceleration processes and non-thermal character of the fusion reactions. Investigation of the location and dynamics of neutrons produced in PF sources is of great importance for the understanding of the fusion reaction character in a plasma pinch [2]. Several models (non-thermal, beam-target, moving boiler, gyrating particle model (GPM)) [3,4] have been considered so far but, still, there is no ultimate experimental evidence supporting one of them. In particular, the mechanisms responsible for deuteron acceleration, the distributions of deuteron energies and directions, the role of magnetic gyration and the spatial extent of the fusion source are still poorly understood [5].

Plasma source imaging is a useful experimental tool that can help to verify various hypotheses on PF fusion models. However, due to the penetrating nature of fast neutrons and the relatively small dimensions of the plasma source, it is difficult to design a neutron pinhole imaging system for PF devices. Over the past few decades several attempts have been made to tackle this problem [6–8].

Because of new technical and experimental possibilities (*i.e.* new types of scintillators, high quantum efficiency photomultiplier tubes, fast acquisitions systems, etc.) as well as modern numerical methods for neutron transport calculations, the problem of the precise spatial and temporal measurement of neutron emission from PF sources is still up to date. The aim of this paper is to present the novel design of the neutron pinhole camera based on small-area plastic scintillation detectors and the work on optimization of its geometrical configuration using MCNP [9] calculations. The camera is characterized by a 5 mm spatial resolution and a few nanoseconds time resolution and will be used for studies of a character of DD fusion reaction in the PF-24 source.

2 PF-24 plasma focus source

The medium scale PF-24 facility has been recently installed at the Institute of Nuclear Physics Polish Academy of Sciences (IFJ PAN), Poland. The system consists of the following main units (fig. 1):

[a] e-mail: jakub.bielecki@ifj.edu.pl

Fig. 1. Plasma focus (PF-24) device at IFJ PAN (Poland).

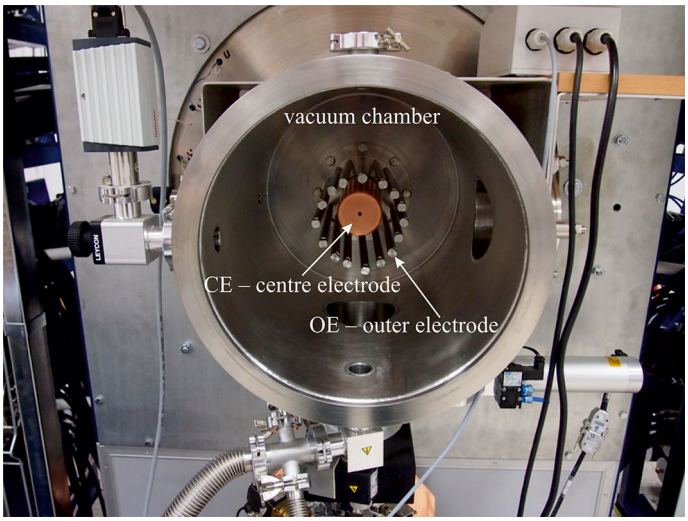

Fig. 2. Geometry of the PF-24 electrodes.

– condenser bank and pulsed electrical power circuit with a collector and low-inductance cables;

– vacuum chamber with coaxial electrodes and pumping and gas handling systems;

– plasma diagnostic and data acquisition system.

The electrical energy is transferred to the collector and electrodes via low-inductance cables. The vacuum chamber, which surrounds the electrodes, has the following dimensions: 360 mm in diameter and 400 mm in length. Two coaxial electrodes are shown in fig. 2. The copper centre electrode (CE) has a radius of 30.5 mm and its length is 165 mm. The outer electrode (OE) (*i.e.* cathode) consists of 16 stainless-steel rods, each 12 mm in diameter. The OE radius of 55 mm is defined as the distance between the axis of CE and the centre of an OE rod. The cylindrical alumina insulator is mounted on the CE. Its main part extends 32.5 mm along the CE into the vacuum chamber. The insulator prescribes the shape of the initial current sheet between the CE and the plasma focus back plate on which the OE rods are fixed.

The condenser bank of capacitance of 116 μF can be charged to the voltage ranging from 16 kV to 40 kV, which corresponds to discharge energies from 15 kJ to 93 kJ. During these experiments, the PF-24 was operated with deuterium gas at a pressure of (201 ± 14) Pa and the capacitors bank was charged to 16 kV. The neutron yield was measured with a beryllium activation counter [10]. Simultaneously, the current signal and the current derivative in the discharge circuit were monitored by a Rogowski coil and a magnetic probe located inside the PF-24 collector.

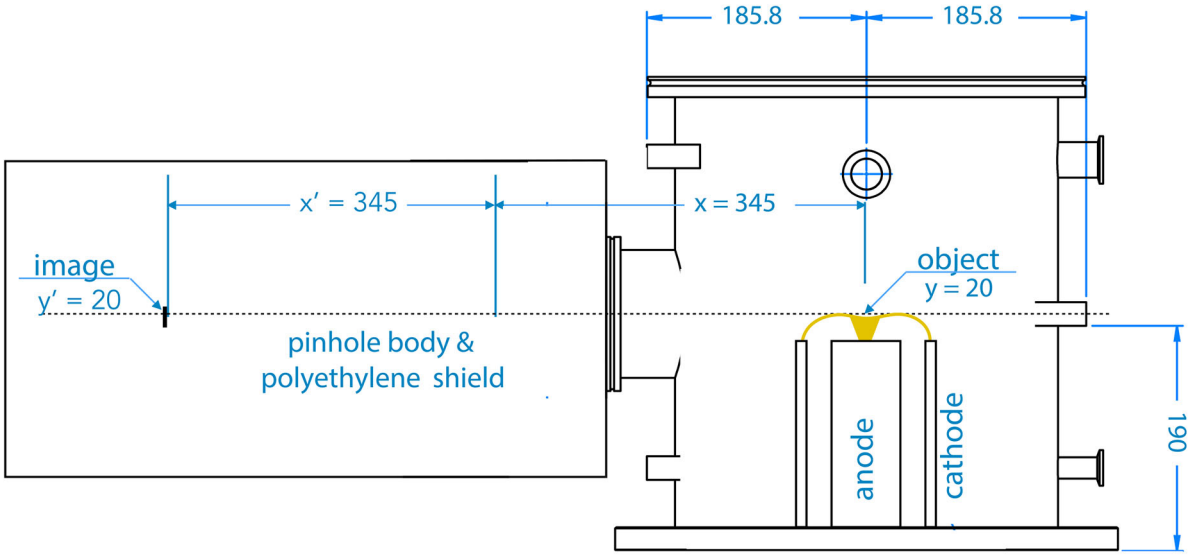

Fig. 3. Geometrical layout of the neutron pinhole camera for the PF-24 source (all dimensions in mm). The PF-24 source is shown on the right-hand side of the figure.

3 Pinhole geometry and design of the detection system

The geometrical layout of the neutron pinhole camera is shown in fig. 3. The camera is composed of the following main parts: (1) the pinhole body consisting of a cylindrical copper collimator with established geometrical parameters, shielded by a layer of cadmium (fig. 4(a)); (2) four linearly arranged BCF-12 scintillation detectors enclosed in a lead box and coupled via 25 m long optical fibres to PMTs (fig. 4(b)); (3) a polyethylene shield which helps to avoid an influence of the scattered neutrons (see fig. 4(a)).

The camera utilizes the principles of standard optical geometry adapted for neutron imaging. The main constrains on the detection system are defined by the following basic parameters:

i) Magnification factor:

$$m = \frac{x'}{x} = \frac{y'}{y}, \tag{1}$$

where x is the source-to-pinhole distance, x' the is pinhole-to-image distance and y and y' are size of the object (plasma column) and size of the image, respectively.

ii) Geometrical blur:

$$D = d\frac{(x + x')}{x} = d(1 + m), \tag{2}$$

where D denotes the size of the image of a point neutron source and d is the diameter of the pinhole.

iii) The neutron fluence at the image plane:

$$F = \frac{Yd^2}{4\pi x^2 y'^2}, \tag{3}$$

where Y is the total neutron yield per discharge emitted from the observed plasma column.

iv) The spatial resolution R, defined as the distance between two point sources whose images are tangential, is given by

$$R = D\frac{x}{x'} = d\left(1 + \frac{1}{m}\right). \tag{4}$$

The dimensions and geometrical layout of the scintillators have been chosen to cover a 2 cm part of the plasma column during the pinch phase at the magnification factor $m = 1$. Such a choice of m defines the total field of view (FOV) of the camera equal to the total area of the detectors (20 mm × 5 mm). The effective aperture of the pinhole has been chosen to $d = 1.7$ mm that defines the spatial resolution of the imaging system $R = 3.4$ mm that is lower than the dimensions of a single scintillator. The image size $y' = 4 \times 5$ mm $= 20$ mm, where 4 is the number of detectors, and the source-to-pinhole distance $x = 345$ mm. Thus, from eq. (3), the fluence at the image plane per $Y = 1$ neutron emitted from the PF-24 source can be estimated as $F \cong 5 \times 10^{-9}$ n/mm^2. It is clear that a compromise between a

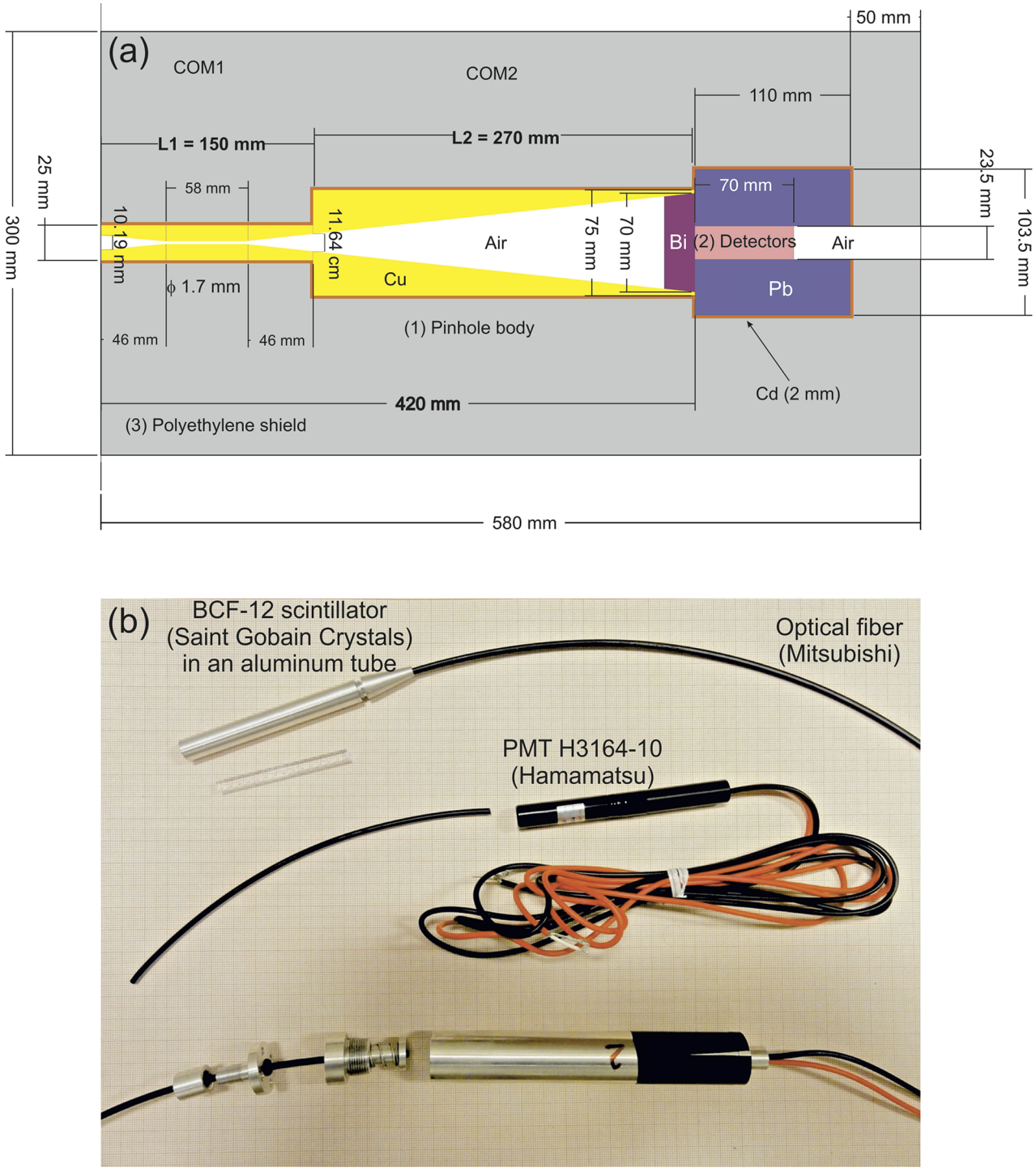

Fig. 4. Main elements of the PF-24 neutron pinhole camera: (a) pinhole body and polyethylene shield; (b) BCF-12 scintillation detector coupled to PMT via optical fibre.

reasonable resolution of the system and the requirement on the number of recorded events for a good statistics is necessary. Assuming that at least 100 neutrons should be registered by the detection system at the image plane, the total neutron yield per discharge of PF-24 source has to be greater than $\sim 2 \times 10^8$ n/discharge (assuming that the detection efficiency = 1). This evaluation has been made only on the basis of simple geometrical considerations and enables a rough estimate of the required sensitivity of the neutron imaging system.

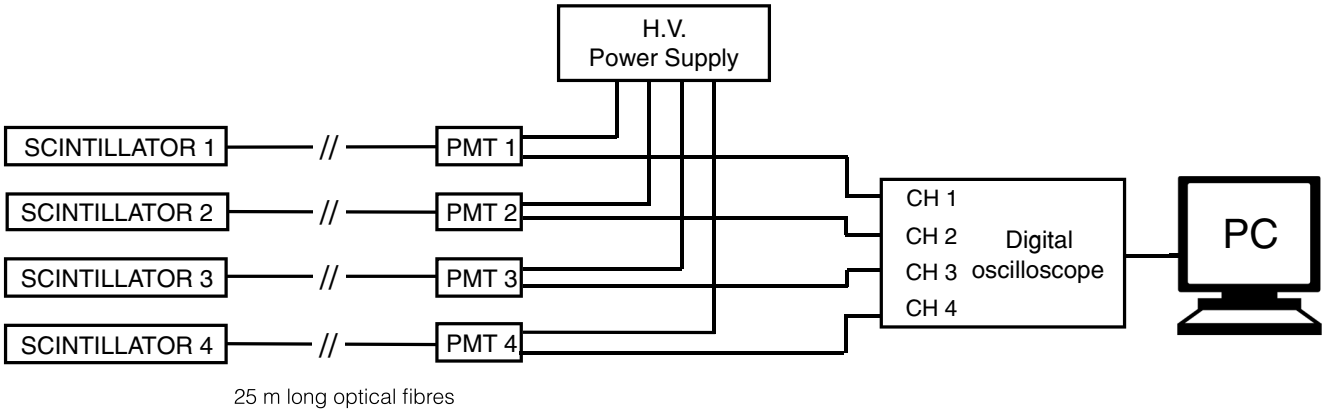

Fig. 5. Block diagram of the detection and acquisition systems for the neutron pinhole camera.

More realistic values can be obtained by tracking the neutron transport processes on the distance between the neutron source and the detector. The simple geometrical evaluation presented above served as a starting point for Monte Carlo calculations conducted in order to design the optimal geometrical layout of the pinhole [11]. The shape and dimensions of the pinhole camera's collimator have been optimized to ensure high-quality collimation and shielding (see sect. 4).

The pinhole camera will be placed at the minimal possible distance from the PF-24 chamber in order to achieve the maximal neutron fluence at the imaging plane. Due to this fact, the separation of emitted X-rays and neutrons by a time-of-flight method is not possible. Therefore, the set of detectors is enclosed in a lead box of 103.5 mm × 110 mm × 87 mm to prevent from passing of the X-rays through the scintillators. This allows reducing the signal from hard X-rays (HXR) emitted from the plasma column of the PF-24 device.

The block diagram of the detection and acquisition system is shown in fig. 5. The main component of the detection system is a set of four closely packed BCF-12 scintillators (Saint Gobain) in the form of 5 mm × 5 mm × 60 mm rods. Such a set of scintillators forms a one-dimensional array. The scintillators consist of a polystyrene based core and a PMMA (poly(methyl methacrylate)) cladding. A titanium paint cladding applied to the scintillator's surface minimizes the loss of photons in the optical system and eliminates an optical crosstalk among closely packed scintillators. The scintillating core contains a combination of fluorescent dopants selected to produce the desired scintillation, optical and radiation-resistance characteristics. PMMA -the standard cladding material for Saint-Gobain Crystals' scintillators- has a density of 1.2 g/cm^3 and refractive index of 1.49. The refractive index of the core (1.60) and cladding and the cross section (square) of the scintillator determine the trapping efficiency, which ranges from 3.4% for events occurring at the scintillator axis to $\sim 7\%$ for events near the core-cladding interface [12]. The scintillator material emits blue light of 435 nm wavelength. The light is transferred via 25 m long optical fibre (Mitsubishi SH 8001) to Hamamatsu H3164-10 photomultiplier tubes (PMT) with a high gain coefficient of 1×10^6. The spatial separation of the scintillation element from the PMT and data acquisition system enables reducing the background noise. Short scintillation decay time of 3.2 ns ensures high temporal resolution of the detection system. The peak sensitivity wavelength of the PMT is 420 nm and is close to the wavelength corresponding to the maximum emission of the light from the BCF-12 scintillators. The bias voltage was applied to PMT cathode from a high voltage power supply (Fast ComTec NHQ202m). The output signals from the PMTs were recorded on a 1 GHz digital oscilloscope (Tektronix DPO5104B) and analyzed using a PC.

4 Optimizations of the pinhole geometrical parameters by means of Monte Carlo calculations

Geometrical parameters of the pinhole camera for fast neutron imaging were established based on Monte Carlo calculations. For this purpose the MCNP code was applied to track neutrons and photons inside the pinhole and shield structure over broad ranges of energies.

In the calculations, the surface tally type (F1) for neutrons and photons was used to determine the number of particles crossing the detectors front faces. The investigated surface was divided into 20 pixels, each having an area of 2 mm^2. In order to obtain only the neutron current flowing into the detector, the cosine card was used. This card enables to restrict the current calculations to be performed within the specified angular ranges —so-called angular bins. The angular bins were defined with respect to the normal to the detection plane and were assumed to be between 0° and 90°. Although the pinhole camera has been designed to register 2.5 MeV neutrons, the influence of scattered neutrons has been also evaluated. For this purpose the energy card was used and the tally was divided into the following energy bins: 0–0.1 MeV, 0.1–0.5 MeV, 0.5–1 MeV, 1–2 MeV and 2–2.5 MeV and the last one for the sum of all energies.

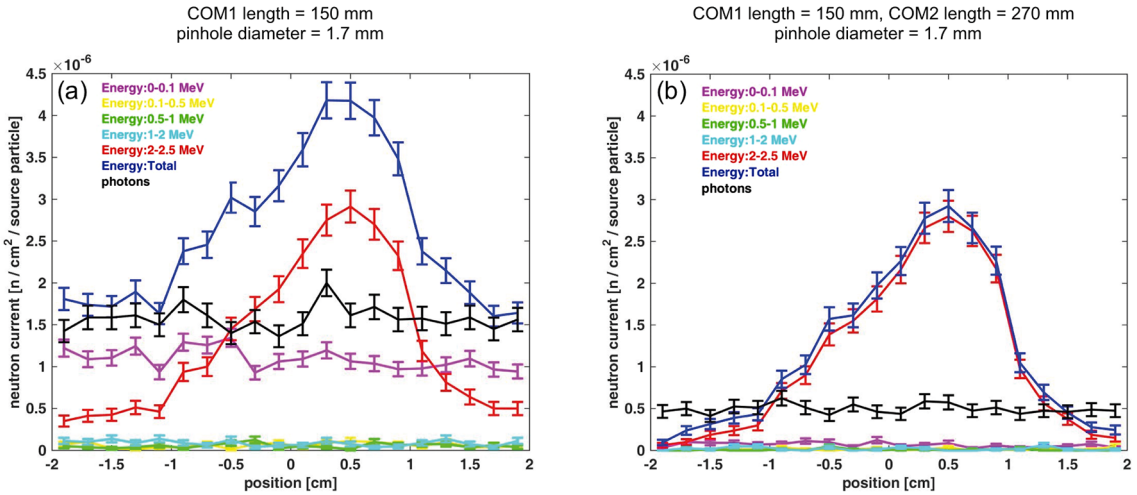

Fig. 6. Neutron current at the image plane per one neutron emitted by the volume source with longitudinally varying intensity S2: (a) case when only COM1 is taken into account; (b) case when COM1+COM2 are taken into account.

The tallies were run for 2×10^9 histories, with each history corresponding to one particle emitted by the source. The maximum relative error for these calculations was lower than 5%.

Based on the set of MC calculation results and after a consideration of the technical capabilities of the PF-24 device, the optimal source-to-pinhole body distance and the outer diameter of the polyethylene shield has been established to 270 mm and 300 mm, respectively.

Despite the fact that the principles of geometrical optics can be also used to fast neutron imaging, the construction of the neutron pinhole camera must be significantly different from the optical one. In particular, a completely different shielding and collimation concept must be applied due to the specific nature of the neutron propagation in the matter. This influences the pinhole length, that must have at least the length of several mean free paths of neutrons in copper ($\sim$ 27 mm) in order to get the required collimation of the neutrons. Moreover, the camera walls should be made of a very good neutron absorber.

Various geometrical configurations of the pinhole have been tested and its optimal parameters have been established [13,14]. As a result, the optimal layout of the pinhole body has been designed to consist of two components (marked in fig. 4(a) as COM1 and COM2): the first one having an outer diameter of 25 mm and a length of 150 mm, the second one having a diameter of 75 mm and a length of 270 mm. The "optical centre" of the set-up is located in the centre of the first pinhole component (COM1).

The geometrical parameters of the pinhole have been investigated by modelling a volume neutron sources consisting of a cylinder of 10 mm in diameter and 20 mm in length assuming: a) uniform intensity (S1), b) longitudinally varying intensity in the following proportions: (1:2:3:5), with the maximum emission of the neutrons shifted off the axis by 0.5 cm (S2). Additionally, a five-point neutron source (equal intensities, 5 mm distance between the points) (S3) has been modelled in order to check the spatial resolution of the pinhole camera.

Because of high background of gamma radiation and relatively high sensitivity of the detectors to X-rays, a set of shields has been designed. A cone-shaped bismuth shield in front of the detectors and a 40 mm thick lead shield around the detectors have been applied. The thickness of the bismuth layer has been arbitrary chosen to be 20 mm, however the modular construction of the second component (COM2) enables, if necessary, to add another layers of the attenuator. To reduce the number of thermal neutrons, which may reach the detectors, the whole pinhole structure and the detectors with the lead shield have been covered by a 2 mm thick cadmium layer (see fig. 4(a)).

Due to the fact that neutrons are scattered in a polyethylene shield, the lower-energy neutrons (below 2 MeV) are present in the set-up and can reach the detectors. Figure 6 shows the neutron current per one particle emitted by the source at the image plane in the case when only the first component of the pinhole (COM1) (fig. 6(a)) or the whole pinhole structure (COM1+COM2) (fig. 6(b)) is taken into account. It is clear that the introduction of COM2 reduces, by factor of $\sim$ 10, the number of scattered, less energetic neutrons (below 0.1 MeV) reaching the detection system. On the other hand, the flux of neutrons within the energy range of 2–2.5 MeV is only slightly reduced inside the structure of the set-up and has a weak influence on the total number of neutrons reaching the detectors. Based on the calculations, the optimal length of the components, in terms of the maximal neutron current at the detection plane for the assumed spatial resolution of the system, was established to be $L1 = 150$ mm and $L2 = 270$ mm for COM1 and COM2, respectively.

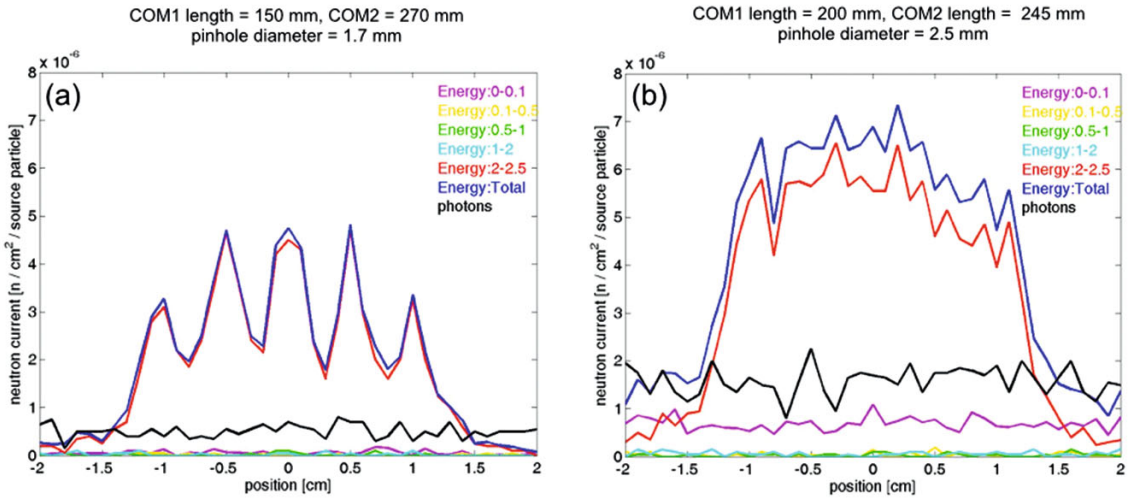

Fig. 7. Neutron current per one source particle at the image plane for the five-point neutron source (S3) for: (a) the chosen geometrical parameters of the pinhole; (b) other considered geometrical configuration of the pinhole camera. The statistical errors (not indicated in the figure for sake of clarity) are comparable to the errors from plots in fig. 6.

Figure 7(a) shows the neutron current per one source particle at the image plane for the five-points neutron source (S3) for the chosen geometrical parameters of the pinhole ($d = 17\,\mathrm{mm}$, $L1 = 150\,\mathrm{mm}$, $L2 = 270\,\mathrm{mm}$). Judging from this figure, the peaks corresponding to five point sources, located 5 mm away from each other, are clearly resolved, thus the spatial resolution of the system is better than 5 mm. A higher spatial resolution of the imaging system is not required since the main limitation on the resolution is connected with the dimensions of the single scintillator. It can be also noted that the neutron currents associated with two images of the outermost sources ($\sim 3.3 \times 10^{-6}\,\mathrm{n/cm^2}$/source particle) are 0.7 times lower than the currents associated with the three remaining images ($\sim 4.7 \times 10^{-6}\,\mathrm{n/cm^2}$/source particle). This effect is caused by the geometrical layout of the pinhole. For comparison, fig. 7(b) presents an exemplary plot of the neutron current per one source particle at the image plane for the five-points neutron source (S3) for other considered geometrical configuration of the pinhole camera ($d = 25\,\mathrm{mm}$, $L1 = 200\,\mathrm{mm}$, $L2 = 270\,\mathrm{mm}$). In this case a much worse spatial resolution is achieved.

In the next step, the total number of neutrons reaching the front face of each detector of the camera per one emitted particle has been calculated. The results for the volume neutron sources (S1) and (S2) are presented in fig. 8(a) and fig. 8(b), respectively. Similarly as for the five point source, a decrease of the neutron current for the outer detectors by about 35% compared to the neutron current measured by the inner detectors is observed. In the case of the longitudinally varying neutron source, the reconstructed neutron currents at the detectors 1–4 have the following ratios: 1:2:3:1.6. The distortions of the neutron source image, that are reflected by the neutron current registered by the outer detectors, are caused by the neutron scattering by the pinhole structure. This observation has to be taken into account during the experiments with PF-24 source.

5 Tests of the BCF-12 plastic scintillation detectors for the neutron pinhole camera

In order to check the response of the detectors to mixed HXR and neutron radiation the detectors were placed end-on (position A) and side-on (position B) to the PF-24 electrodes axis at the distance of 2 m. At the same time all four scintillators were enclosed in a Pb shield preventing from passing of HXR to the detectors' side faces. Additionally, 20 mm thick Bi plate was placed in front of the scintillators in order to reduce the signals from X-rays. Figures 9(a) and (b) present the exemplary scope traces of HXR and neutron signals collected by the BCF-12 plastic scintillation detectors at the positions A (discharge no. 1410080) and B (discharge no. 14101004), respectively. The corresponding plots of $I(t)$ and $\mathrm{d}I/\mathrm{d}t(t)$ signals measured by the Rogowski coil and magnetic probe are shown in figs. 10(a) and (b). The parameters of the discharges for the traces were the following: charging voltage $U_0 = 16\,\mathrm{keV}$, pressure of the deuterium filling gas $p_0 = 200\,\mathrm{Pa}$. The neutron yields measured by Be counter were 5.65×10^9 and 8.82×10^8 n/discharge for the discharge no. 14100805 and 14101004, respectively. The first peak of signals is due to HXR produced by the interaction of energetic electrons with the copper anode. The second peak results from the detection of the neutrons emerging from the fusion reaction. It is delayed with regard to the first peak because of the difference in the time of flight between the neutrons and hard X-rays.

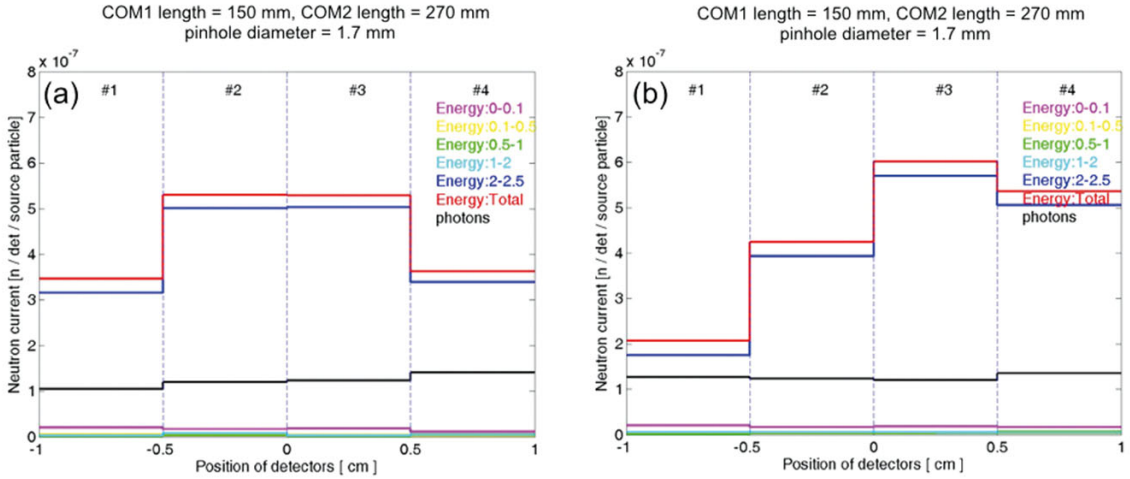

Fig. 8. Number of neutrons reaching the front faces of the detectors of the pinhole camera for: (a) volume source with a uniformly spread neutron emission intensity (S1); (b) volume neutron source with a longitudinally varying intensity of neutron emission (S2).

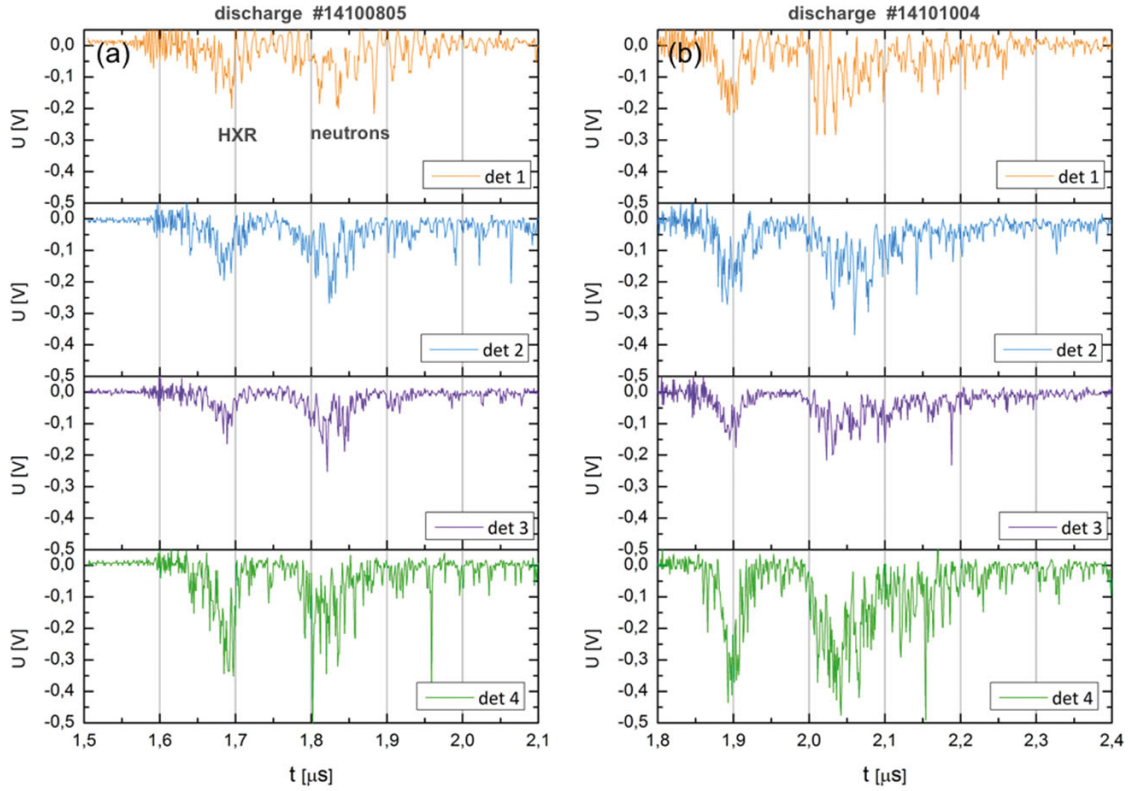

Fig. 9. Oscilloscope traces of HXR and neutron signals collected by the scintillation detectors: (a) end-on (position A); (b) side-on direction (position B) for pulse #14100805 and pulse #14101004, respectively.

Additionally, a correlation between the total neutron yield measured by means of Be counter and the signals from the scintillation detectors was investigated in order to compare the relative efficiencies of each detection channel. For this purpose, the detectors were subsequently placed inside a 10 cm ×10 cm × 5 cm lead block with a hole of 1 cm in diameter. The detectors were located at the distance of 2 m from the PF source, parallel to the electrode axis. The neutron signals registered by the scintillation detectors were recorded on the multichannel oscilloscope for several discharges with different neutron yields. Then, the signals were integrated over time. The integrated signals were plotted as a function of the total neutron yield measured by the Be counter. Results for detectors 1–4 are presented in fig. 11. Determination coefficients R^2 for the linear fits presented in fig. 11 are: ${R_1}^2 = 0.983$ for detector 1, ${R_2}^2 = 0.972$

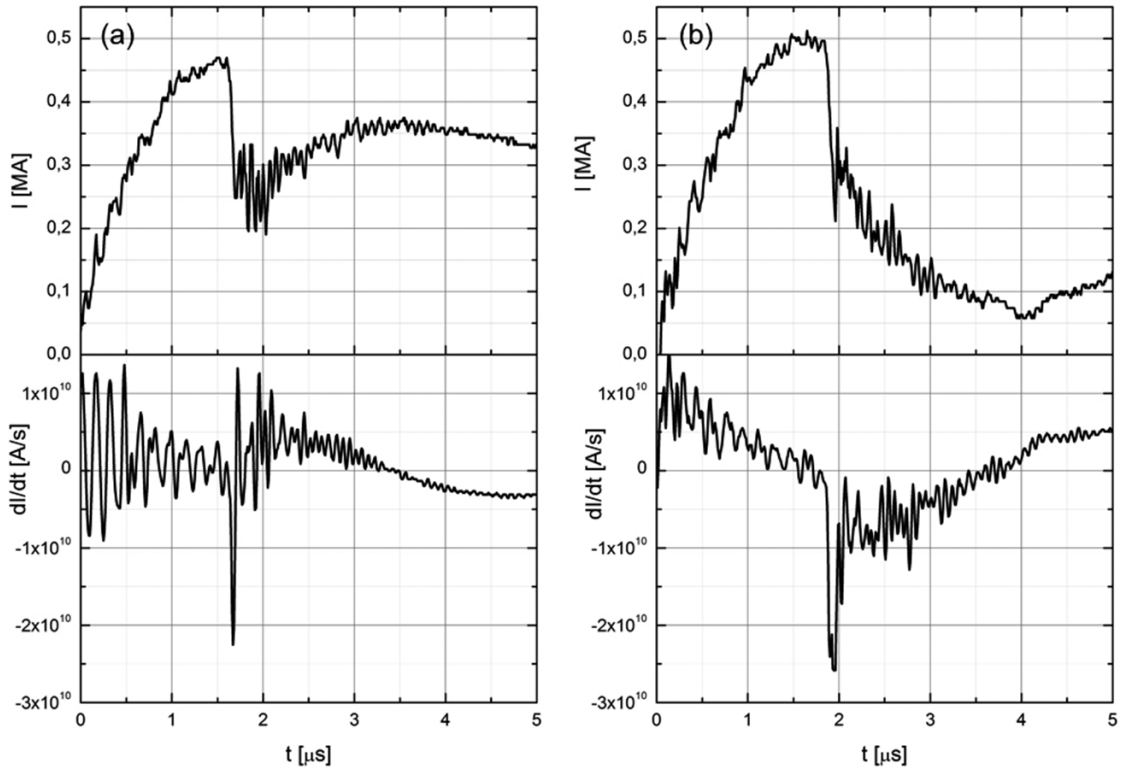

Fig. 10. Current signal measured by Rogowski coil (upper panels) and dI/dt signal measured by the magnetic probe of PF-24 (lower panels) for: (a) pulse #14100805; (b) pulse #14101004.

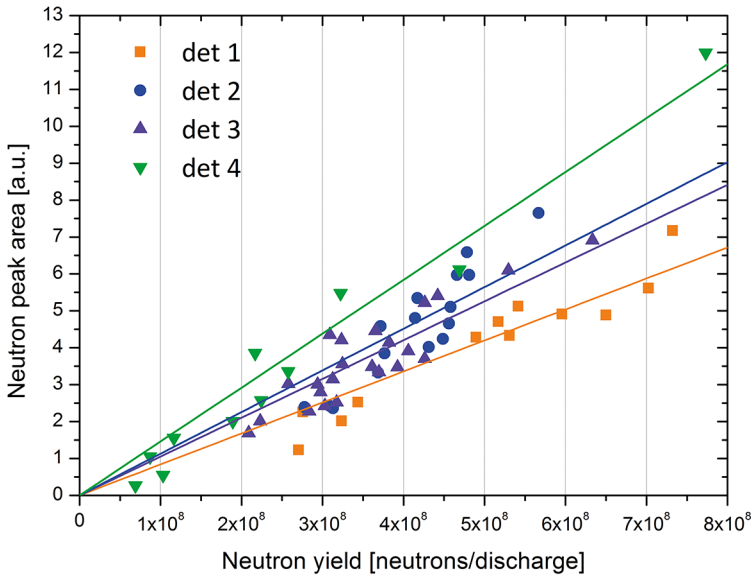

Fig. 11. The integrated signals from the scintillation detectors 1–4 as a function of the total neutron yield measured by the Be counter.

for detector 2, ${R_3}^2 = 0.977$ for detector 3 and ${R_4}^2 = 0.979$ for detector 4. The slopes of the linear fits for detectors 1–4 are, respectively: $\alpha_1 = 8.40 \times 10^{-9}$ [a.u.], $\alpha_2 = 1.12 \times 10^{-8}$ [a.u.], $\alpha_3 = 1.05 \times 10^{-8}$ [a.u.] and $\alpha_4 = 1.46 \times 10^{-8}$ [a.u.]. These results show that the efficiencies of the detectors are slightly different. Although the design of each of the detectors was the same, even little differences in the technological process of the scintillator and optical fibre bonding can lead to the observed discrepancies. Also, the individual features of the PMTs and scintillators can influence, to some extent, the efficiency of each detection channel. However, the efficiencies of the channels can be adjusted by the proper gain matching. Moreover, these results allow for evaluation of the number of neutrons registered by the

scintillation detectors during the routine experiments with the neutron pinhole camera, providing that the absolute efficiency of the detectors is known. Among 62 analysed discharges, 57 had the total neutron yield measured by the Be counter above 2×10^8 n, which is required to register at least 100 neutrons by the detection system, assuming a 100% detection efficiency. It should be stressed that during these tests the PF source was operated at the charging voltage of 16 kV while the maximum of the voltage for this device was 40 kV. Notwithstanding the systematic research already done with PF-24, the optimization of the device as a neutron source has not been studied in detail. After the optimization of the device in terms of the charging voltage and filling gas pressure, higher neutron emission is expected.

6 Conclusions

The neutron pinhole camera dedicated for investigations of the spatial and temporal distribution of neutrons emitted from plasma column of the PF-24 source has been designed.

The pinhole structure composed of two copper conical collimators and a cylindrical entrance of 58 mm length enclosed in polyethylene shield was design by means of geometrical considerations and MCNP neutron transport computations. Such a design of the pinhole structure ensures a good collimation of 2.5 MeV neutrons as well as effective reduction of thermal neutron current and X-ray contamination.

Four small-area BCF-12 scintillation detectors coupled to PMTs that serve as the detection system of the camera have been chosen, constructed and then tested in the mixed radiation field of the PF-24 plasma focus source. The detectors allow to obtain a spatial resolution of 5 mm and a temporal resolution of a few nanoseconds, which make them suitable detection system for the neutron pinhole camera. Preliminary results show that the efficiency as well as temporal and spatial resolution of the detection system are satisfactory for imaging of the plasma pinch in the PF-24 device. The main technical challenge is the spatial separation of the scintillation element from the PMT and data acquisition system that allows reducing the background noise. It requires an excellent optical bonding of the fibre and the scintillator. The technique of bonding seems to have a significant influence on the performance of the detectors.

The traces collected from the scintillation detectors feature signals related to HXR and neutrons emissions. However, during the routine experiments with the neutron pinhole camera, the pinhole structure together with the detection system will be placed at the minimal possible distance from the PF-24 chamber. This will ensure the maximal neutron fluence at the imaging plane of the camera. In this case the HXR/neutron signal separation by time-of-flight method is not possible. Thus, the detectors have to be completely shielded against HXR using Pb and Bi attenuators.

To summarize, the neutron pinhole camera for PF-24 device has been designed and all necessary steps to optimize the system in terms of neutron detection efficiency, spatial resolution and background reduction have been performed. Based on the calculations and experiments presented in the article a prototype of the camera has been already constructed. An experiment dedicated to imaging of PF-24 neutron source in order to study the fusion reaction mechanisms is already planned and will be performed.

The work has been performed within the framework of the strategic research project "Technologies supporting development of safe nuclear power engineering" financed by the National Centre for Research and Development (NCBiR). Research task "Research and development of techniques for the controlled thermonuclear fusion", Contract No. SP/J/2/143234/11. The authors gratefully acknowledge the assistance of Mr. W. Janik and Mr. M. Turzański in development and testing of the small-area scintilation detectors.

References

1. F. Castillo-Mejía, I. Gamboa-de Buen, J.J.E. Herrera-Velázquez, J. Rangel-Gutiérrez, J. Phys. Conf. Ser. **511**, 012021 (2014).
2. M. Zakaullah, I. Akhtar, G. Murtaza, A. Waheed, Phys. Plasmas **6**, 3188 (1999).
3. F. Castillo-Mejía, J.J.E. Herrera-Velázquez, J. Rangel-Gutierrez, AIP Conf. Proc. **563**, 258 (2001).
4. U. Jager, H. Herold, Nucl. Fus. **27**, 407 (1987).
5. S.V. Springham, A. Talebitaher, P.M. Shutler, S. Lee, R.S. Rawat, P. Lee, Appl. Phys. Lett. **101**, 114104 (2012).
6. R.W. Bauer, R.C. Weingart, *Proceedings of the Conference on Diagnostics of High Temperature Plasmas* (Oak Ridge National Laboratory, Oak Ridge, TN, 1976).
7. D.R. Slaughter, *Proceedings of the 1978 Nuclear Science Symposium* (Washington, D.C., 1978).
8. K. Steinmetz, K. Hübner, J.P. Rager, B.V. Robouch, Nucl. Fus. **22**, 30 (1982).
9. X-5 Monte Carlo Team, *MCNP – A General Monte Carlo N-Particle Transport Code Version 5*, Report no. LA-UR-03-1987 (Los Alamos National Laboratory, 2003).

10. B. Bieńkowska, R. Prokopowicz, M. Scholz, *Beryllium neutron activation counter for pulsed DD fusion sources*, IFJ Report no. 2064/AP (2013) available on-line: `http://www.ifj.edu.pl/publ/reports/2013/`.
11. M. Scholz, J. Bielecki, A. Wójcik-Gargula, U. Wiącek, K. Drozdowicz, A. Igielski, A. Kulińska, G. Tracz, U. Woźnicka, *Assumptions for the design of a neutron pinhole camera dedicated to the PF-24 device*, IFJ Report no. 2073/AP (2014) available on-line: `http://www.ifj.edu.pl/publ/reports/2014/`.
12. J. Gearhart, *Investigation of BCF-12 plastic scintillating coherent fiber bundle timing properties*, PhD thesis (Air Force Institute of Technology, Ohio, 2012).
13. U. Wiącek, *Optimization of the design of the fast neutron imaging pinhole camera at the PF-24 Plasma Focus device – Monte Carlo modelling*, to be published in IFJ report.
14. U. Wiącek, J. Bielecki, A. Igielski, M. Scholz, A. Wójcik-Gargula, *MCNP simulations for optimization of the pinhole camera for fast neutrons imaging*, to be published in Nucl. Instrum. Methods A.